Critical role of lysosomes in the dysfunction of human Cardiac Stem Cells obtained from failing hearts☆

Giuseppe Gianfranceschi [a,1,2], Angela Caragnano [a,1,2], Silvano Piazza [b,2], Ivana Manini [a,2], Yari Ciani [b,2], Roberto Verardo [b,2], Barbara Toffoletto [a,2], Nicoletta Finato [a,2], Ugolino Livi [c,2], Carlo Alberto Beltrami [a,2], Giacinto Scoles [a,2], Gianfranco Sinagra [d,2], Aneta Aleksova [d,2], Daniela Cesselli [a,*,2], Antonio Paolo Beltrami [a,*,2]

[a] Department of Medical and Biological Sciences, University of Udine, Udine, Italy
[b] Laboratorio Nazionale Consorzio Italiano Biotecnologie (LNCIB), Trieste, Italy
[c] Department of Experimental Medical and Clinical Sciences, University of Udine, Udine, Italy
[d] Cardiology Department, University of Trieste, Trieste, Italy

ARTICLE INFO

Accepted 20 April 2016

Keywords:
Stem cells
Heart failure
Lysosome
TFEB
Cell senescence

ABSTRACT

The in vivo reparative potential of Cardiac Stem Cells (CSC), cultured from explanted failing hearts (E-), is impaired by cellular senescence. Moreover, E-CSC are characterized, with respect to CSC obtained from healthy donors (D-), by an arrest in the autophagic degradation. Although the lysosome plays a pivotal role in cellular homeostasis and defects of this organelle may be associated with aging and heart failure, the lysosomal function of CSC has never been investigated. The aim of this work was to focus on the Lysosomal Compartment (LC) of E-CSC, evaluating elements that could jeopardize lysosome functionality.

Methods and results: Bioinformatics analysis conducted on genes differentially expressed between D- and E-CSC identified lysosomal-related gene sets as significantly enriched. Moreover, 29 differentially expressed genes were part of CLEAR (Coordinated Lysosomal Expression and Regulation) gene network, by which Transcription Factor EB (TFEB) regulates cellular clearance. Consistently, live cell imaging and flow cytometry analyses showed that the lysosomes of E-CSC are less acidic than the D-CSC ones. Furthermore, confocal microscopy showed in E-CSC: an accumulation of intralysosomal lipofuscins, a reduction of cathepsin B activity, evidence of lysosome membrane permeabilization, and the reduction of the nuclear active TFEB. The use of Rapamycin (TORC1 inhibitor) was able on one hand to increase TFEB activation and, on the other hand, to reduce lipofuscin mass, potentiating the lysosomal functionality.

Conclusions: This study demonstrated for the first time that E-CSC are characterized by a blunted activation of TFEB and an altered proteostasis. TORC1 hyperactivation plays a central role in this phenomenon.

Abbreviations or acronyms

CSC	Cardiac Stem Cells
D-CSC	Cardiac Stem Cells isolated from Donor hearts
E-CSC	Cardiac Stem Cells isolated from Explanted, failing hearts
HF	Heart failure
LC	Lysosomal Compartment
LV	Left ventricle
AO	Acridine orange

1. Introduction

Cellular senescence is a cellular condition characterized by a stable arrest of the cell cycle coupled with stereotyped phenotypic changes

☆ Grant support: Project ERC-7FP SP 2 IDEAS QUIDPROQUO G.A. n. 269051 (G.S., D.C., A.P.B., G.G.). Italian Ministry of Research and Technology, FIRB accordi di programma 2011 n. RBAP11ETKA_007 (A.P.B). The funders had no role in study design, data collection and analysis, decision to publish or preparation of the manuscript.

* Corresponding authors at: Istituto di Anatomia Patologica, Università degli Studi di Udine, P.zzle S. Maria della Misericordia, 33100 Udine, Italy.
E-mail addresses: daniela.cesselli@uniud.it (D. Cesselli), antonio.beltrami@uniud.it (A.P. Beltrami).

[1] Giuseppe Gianfranceschi and Angela Caragnano equally contributed to the paper.
[2] This author takes responsibility for all aspects of the reliability and freedom from bias of the data presented and their discussed interpretation.

[1]. Increasing evidence shows a cause–effect correlation among cellular senescence, aging, and cardiovascular disease, including heart failure (HF) [2]. This correlation involves human Cardiac Stem Cells (CSC) too. Indeed, we recently demonstrated that senescent CSC isolated from explanted ischemic hearts (E-CSC) are unable to protect in vitro rat adult cardiac myocytes, exposed to Simulated Ischemia/Reoxygenation (SI/RO), from apoptosis and senescence. When compared with healthy donor heart-derived CSC (D-CSC), E-CSC are characterized by a blunted ability to stimulate a reparative healing of the infarcted mouse heart [3]. By analyzing the molecular pathways connected with CSC senescence, we found, inter alia, that the hyperactivation of the mTOR Complex 1 (mTORC1), followed by a block in the autophagic flux, plays a crucial role in the dysfunction of E-CSC [3]. However, the specific contribution played by the Lysosomal Compartment (LC) in the senescence of this cell type has not been elucidated yet.

The LC is considered to be the final destination of every intracellular degradative pathway (i.e. autophagy, endocytosis, and phagocytosis), with the only exception of the ubiquitin-proteasome system [4]. Lysosomes are eukaryotic, membrane-enclosed, organelles, containing more than 80 different acid hydrolases (i.e. proteases, lipases, nucleases, glycosidases, phospholipases, phosphatases and sulfatases) that are able to degrade an array of biological polymers at an optimal pH of 4.5. This latter is guaranteed by proton pumps (vacuolar ATPase) that reside in lysosomal membranes and is responsible for maintaining the concentration of intralysosomal H^+ 100-fold higher than that of cytosol [4,5]. Besides the degradation, lysosomes are also responsible for other relevant activities including: programmed cell death [6] and exocytosis. This latter is useful to eliminate toxic substances from the cell [7], to release cellular products such as cytokines [8], and to repair the plasma membrane in both normal and pathological conditions [9].

Given that the cellular needs of lysosomal activity significantly change as a function of variables such as the tissue type, the organism age, and the environment, many lysosomal genes exhibit coordinated behavior and are regulated by Trascription Factor EB (TFEB) [10]. This latter is one member of the microphthalmia Transcription Factor (Mit/TFE, subfamily of transcription factors basic Helix–Loop–Helix, bHLH, leucine zipper) family, and is a master gene that positively regulates genes belonging to the CLEAR (Coordinated lysosomal Expression and Regulation) network targeting, among others, genes encoding for lysosomal hydrolases, lysosomal membrane proteins and components of the vacuolar H^+-ATPase (V-ATPase) [10]. To date, 471 genes are identified as TFEB direct targets and represent essential components of the CLEAR network [11]. The study of the functional meaning of these genes clarified that TFEB, through the CLEAR network, regulates lysosomal biogenesis, lysosomal degradation proficiency, autophagy, and other lysosomal-related functions, such as exocytosis, endocytosis, phagocytosis and immune response [11]. In this manner TFEB controls all the paths in which lysosomes are involved in cellular clearance [7,10,11,12,13]. TFEB participates also to a lysosome adaptation mechanism that enables cells to respond both to nutrient conditions and to lysosomal stress by interacting with mTORC1 on the lysosome membrane. Indeed, in the absence of lysosomal stress and in nutrient rich conditions, activated mTORC1 is recruited to the lysosome surface, where it transiently binds to and phosphorylates TFEB, inhibiting its nuclear translocation [14].

Growing evidences report that animal health- and life-span are related to the ability of organisms to respond to stress [15]. Specifically the capability of cells to prevent senescence depends on their efficiency in avoiding the accumulation of damaged macromolecules and organelles and so, on their LC [16]. In line, a defect in the Lysosomal Associated Membrane Protein 2 (LAMP2) is characterized by muscle weakness and cardiomyopathy in mice and Danon disease in patients [17]. Moreover, aging is accompanied by a reduced renewal of cardiomyocytes due to a reduction in both the differentiation of stem cells into cardiac myocytes, and in the division of these latter [18,19]. As a result, undigested lipids, metals, and oxidatively modified proteins accumulate in the cells, in the form of autofluorescent pigments (lipofuscins), which are hardly degraded by the lysosomal hydrolases. The age-related deposition of lipofuscin progressively reduces degradative potential of lysosomes, reducing their ability to fuse with autophagosomes, thus impairing the autophagic flux [20]. Specifically, aged, lipofuscin-rich cardiac myocytes become overloaded with damaged mitochondria, leading to increased oxidative stress, apoptotic cell death, loss of myocardial tissue, and finally development of HF [21]. As a consequence, the proper operation of LC appears to be crucial in the progression of aging.

For the reasons described above, the aim of the present study was firstly, to monitor the efficacy of LC in senescent CSC isolated from end-stage failing hearts. After the demonstration that a dysfunctional LC characterized these cells, we identified the causes of this dysfunction and finally tested a drug-based strategy to interfere with them.

2. Materials and methods

2.1. Patient enrollment and ethical approval

In this study, patients with end-stage heart failure (Stage D AHA classification) who underwent cardiac transplantation, at the University Hospital of Udine, were enrolled as in [3].

The study was approved by the Ethics Committee of Udine (2 August 2011, reference number 47831) in accordance with the Declaration of Helsinki and written informed consent was obtained from each enrolled patient.

2.2. CSC isolation, culture and treatment

Atrial samples were collected both from donor hearts ($n = 14$) and from explanted hearts ($n = 13$) of ischemic patients undergoing cardiac transplantation at the University Hospital of Udine. Table 1 summarizes the demographic and anatomic characteristics of enrolled subjects.

Human CSC were isolated, as in [22,23]. Specifically, atrial samples were first minced with a scalpel. Subsequently, myocardial fragments (≈ 1 mm^3 in size) were enzymatically dissociated incubating them in a 0.25% Collagenase type II solution (Worthington Biochemical Corporation) in Joklik modified Eagle's Medium (Sigma-Aldrich) for 15–20 min at 37 °C. The enzyme activity was stopped by the addition of 0.1% bovine serum albumin (BSA, Sigma-Aldrich) solution in Joklik modified Eagle's Medium (Sigma-Aldrich). The cell suspension was first centrifuged at 100 g for 1 min to remove myocytes and subsequently at 500 g for 5 min. The resuspended pellet was filtered through a pre-wet strainer whose pore size is 40 μm (BD Falcon). The filtered suspension was centrifuged at 500 g for 5 min. Pelleted cells were finally plated at a concentration of $1.5 \cdot 10^6$ in a 100-mm dish and subcultured as in [3]. All the experiments were done at the fourth passage in culture.

Table 1
Demographic and anatomical data of the 27 enrolled subjects. *Data are expressed as mean ± SEM. LV = left ventricle. N.S. = not significant.

	Explanted patients	Controls	*p*
Sample size (n)	13	14	
Age (years)*	64 ± 7	49 ± 11	<0.0001
Sex (male/female)	11/2	7/4	N.S.
Heart weight (g)*	519 ± 88	–	–
Inner LV diameter (cm)*	10 ± 95	–	–
External transverse diameter (cm)*	13 ± 0.9	–	–
Inner longitudinal LV diameter (cm)*	10 ± 0.9	–	–
Anterior LV thickness (cm)*	1.1 ± 0.6	–	–
Lateral LV thickness (cm)*	1.2 ± 0.3	–	–
Posterior LV thickness (cm)*	0.9 ± 0.5	–	–
Septum thickness (cm)*	1.0 ± 0.4	–	–

Summary of the main demographic characteristics of the 27 subjects whose hearts were included in the study. For the explanted patients, anatomical data of the explanted organs, collected by an expert pathologist at the time of transplantation, are also provided. The column *p* indicates the significance of the comparison of age and gender distributions between patients and controls.

For the pharmacologic treatment, E-CSC were exposed to 10 nM Rapamycin for three days. As a control, cells were treated with the vehicle alone (dimethyl sulfoxide, DMSO, Sigma-Aldrich). Vehicle-treated and drug-treated cells were then switched for 24 h to a drug-free medium and subsequently properly assayed in the in vitro experiments.

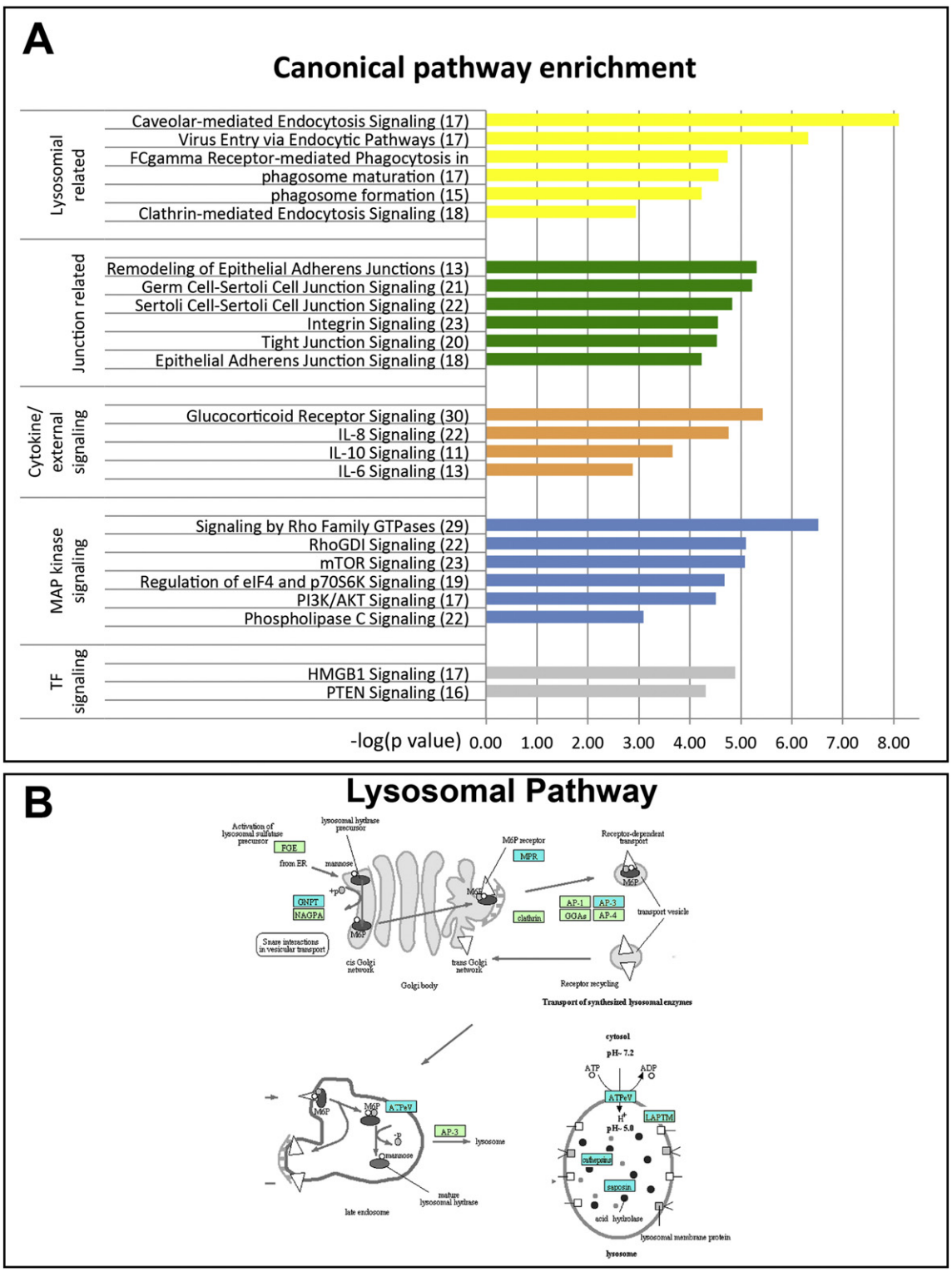

Fig. 1. Bioinformatic analyses of genes differentially expressed by D- and E-CSC. Enriched pathways for the differential expressed genes in the D- and E-CSC comparison (A). Bar-plots graphically represent the results of enrichment tests for the differential expressed genes in the D- and E-CSC comparison; the length is proportionally to the enrichment score (a logarithmic transformation of the *p* value calculated with default parameters in the core analysis (Ingenuity pathway analysis) associated with the specific canonical pathway. The number of differential expressed genes belonging to each specific pathway is also reported. KEGG Map of Protein Processing in Lysosomal Pathway – ko04142 – (B). The map illustrates a modified version of the Protein processing in Lysosomal Pathway and blue rectangles underline genes that are differentially expressed between E-CSC compared with D-CSC.

2.3. Transcriptional profile and functional annotation analysis

The transcriptional profile of CSC obtained from age- and sex-matched donor and explanted hearts (n = 4 each) were analyzed using LNCIB 28K cDNA microarray slides (supporting 28,000 cDNA clones). Original gene expression data obtained in [2] was integrated with a new pair of D- and E-CSC and reanalysed according to last version of gene annotation (http://www.ncbi.nlm.nih.gov/gene). The differential gene expression between CSCs obtained from donor and explanted hearts was established by functions and methods implemented in the *limma* packages (R(version 3.1.2)/Bioconductor (version 3.0). Only Genes that showed a significant ($p < 0.05$) expression difference of at least 0.7 logarithmic fold change (lfc) between D- and E-CSC were considered.

Differentially expressed gene lists were subjected to functional analysis using two different strategies: a) using the Core Analysis function included in IPA (Ingenuity Pathway Analysis, QIAGEN Redwood City, http://www.qiagen.com/ingenuity). The advantage of Ingenuity is that it classifies the genes implicated in each function within sub-functions directly linked to each molecule by bibliographic findings. Both up- and down-regulated identifiers were defined as value parameters for the analysis. After the analysis, generated networks, biofunctions and the canonical pathways were ordered by the statically significance score ($-\log p$-value). B) using the enrichment analysis methods clusterProfiler [24] implemented in R(version 3.1.2)/Bioconductor (version 3.0); the latter tool automates the process of biological-term classification and the enrichment analysis of gene clusters. Specifically clusterProfiler functions enrichGO and enrichKEGG were used to calculate enrichment test for Gene Ontology [25] (GO), terms related to biological processes, molecular functions, and cellular components and Kyoto Encyclopedia of Genes and Genomes (KEGG) [26] pathways; the pathway shown in Fig. 1 was created modifying the Lysosomal pathway from KEGG obtained using Pathview (http://pathview.r-forge.r-project.org/) [27] and integrating gene expression data. In order to further support this findings we calculated and verified the enrichment for a lysosome gene set (n = 170, hypergeomtetric test $p < 0.005$ Supplementary Table S5) that we created using the advanced search function in IPA (since a lysosome gene set is not present in the database).

To assess the presence of TFEB gene targets, R(version 3.1.2) environment was used to match differentially expressed gene lists with a list of 471 identified TFEB direct gene targets [11].

2.4. Flow cytometry analysis

Growing cultures of CSC were detached from the culture substrate with TrypLE Express solution (Gibco — Life Technologies). Detached cells were washed to discard the detaching agent, resuspended in 200 μl of calcium and magnesium free Phosphate Buffered Saline (PBS) and then appropriately stained.

Lysosomal Compartment (LC) was evaluated, in terms of size or functionality, incubating detached cells (1×10^5 cells) 2 h at 37 °C with 75 nM LysoTracker Red DND-99 (Life Technologies), or 15 min at 37 °C with 1 μM Acridine Orange (AO, Sigma-Aldrich), respectively. Both the dyes were diluted in Opti-MEM (Life Technologies). After incubation, cells were washed, resuspended in 500 μl of PBS and analyzed.

Cell analysis was carried out with a FACSCanto analyzer (Becton Dickinson). Cells of interest were gated on the basis of their physical parameters (SSC and FSC). Cell doublets were gated out plotting fluorescence area vs. width. Mean fluorescence intensity was computed by dividing the mean fluorescence of labeled cells by the mean fluorescence of the negative control. The number of different D-CSC and E-CSC lines employed in each experiment is reported in the respective figure legend. For each cell line, experiments were performed in duplicate and at least 10.000 cells per replica were analyzed.

2.5. Fluorescence imaging

Vital staining of CSC with 75 nM LysoTracker Red DND-99 (Life Technologies), or 1 μM Acridine Orange (Sigma-Aldrich), was performed incubating living CSC at 37 °C with the specific dye for 2 h or 15 min, respectively. Both the dyes were diluted in Opti-MEM (Life Technologies). After incubation, CSC were fixed for 20′ at room temperature (RT), with PBS—4% (wt/vol) paraformaldehyde (PFA, Sigma-Aldrich). Fixed cells were stained with 1 μg/ml of 4′, 6-diamidino-2-phenylindole (DAPI, Sigma-Aldrich) diluted in PBS, or permeabilized 10 min at RT, with PBS—0.1% (wt/vol) Triton-X 100 (Sigma-Aldrich) and then stained with primary antibody as described below. We additionally performed vital staining of CSC by incubating living cells with a 10 μM solution of the pH sensitive dye Lysosensor Blue (ThermoFisher) in culture medium for 2 h at 37 °C, 5%CO_2. After incubation, cells were washed with sterile PBS and analyzed with a Leica TCS SP2 Confocal microscope (Leica microsystems) equipped with 63X water-immersion objective. Furthermore, Cathepsin B activity was assayed with the VIVAProbe lysosome assay kit (VIVA Bioscience, UK), following the supplier's protocol. Briefly, adherent cultures of CSC were incubated with diluted Cathepsin B substrate staining solution for 1 h at 37 °C, 5% CO_2 in the dark, washed with PBS and counterstained with 0.5% v/v Hoechst 33342 for 10 min at 37 °C. At the end of the staining procedure, images were collected employing a Leica DMI 6000B live cell imaging setup (Leica microsystems) equipped with a 63X oil-immersion objective (numerical aperture: 1.40).

For immunofluorescence analyses, cultured cells, fixed with PBS—4% (wt/vol) PFA and permeabilized with PBS—0.1% (wt/v) Triton-X 100, were incubated with the following antibody or combination of antibodies: anti-LAMP-2 to mark lysosomes; anti-Galectin 3 in combination with anti-LAMP-2 to evaluate damaged lysosomal membranes; anti-TFEB to evaluate transcription regulation of CLEAR gene network. Cells were then incubated with the appropriate labeled secondary antibody/ies. Nuclei were finally counterstained by DAPI. All the information concerning antibodies used, their dilution, incubation time and temperature are reported in supplementary Table S1.

The number of different D-CSC and E-CSC lines employed in each experiment is reported in the respective figure legend. For each cell line, experiments were performed in duplicate and at least 200 cells per replica were analyzed.

2.6. Immunofluorescence, confocal imaging, quantitative analysis of fluorescence, and spectral analysis

Images of immunofluorescently labeled cells were acquired with a Leica TCS SP2 Confocal microscope (Leica microsystems) equipped with 63X oil-immersion objective (numerical aperture: 1.40). Scrupulous care was taken to keep constant all the acquisition parameters. A quantitation of the total fluorescence of lysosomal lipofuscin, lysosomal Galectin 3 and nuclear TFEB stainings were obtained employing ImageJ software [28]. A threshold was applied to LAMP-2 or DAPI images both to measure colocalization areas and to create a mask to measure the average intensity of lipofuscin autofluorescence or TFEB fluorescence. Lipofuscin and TFEB Integrated Fluorescence Intensity (IFI) was computed for each LC or nucleus multiplying each involved area for the respective mean gray value of lipofuscinor TFEB respectively. Regarding Galectin-3 *punctae*, we quantified the fraction of cells characterized by the presence of colocalization of Galectin-3 and LAMP2.

Autofluorescence emission spectra of lipofuscins were evaluated performing a λ-scanning by confocal microscopy. Unstained samples were excited with a laser emitting at $\lambda = 514$ nm. Fluorescence emission was sampled collecting images between 528 nm and 688 nm with a step of ≈ 5 nm.

The number of different D-CSC and E-CSC lines employed in each experiment is reported in the respective figure legend. For each cell line, experiments were performed in duplicate and at least 200 cells per replica were analyzed.

Adobe Photoshop software was utilized to compose, overlay the images and to adjust contrast (Adobe).

2.7. Western blotting

Whole-cell extract proteins were obtained by lysis of the cells in Radio-Immunoprecipitation Assay Buffer (NaCl 150 mM, 25 mM Tris–HCl, pH 7.6, 1% IGEPAL, 0.1%SDS, 1% SodiumDeoxycholate, 1 mM dithiothreitol, 1 mM Na_2 VO_4, 1 mM Sodium Fluoride, 0.5 mM Phenylmethanesulfonyl fluoride, Protease Inhibitor Cocktail, all from Sigma) for 40 min on ice and centrifugation at 10,000*g*, 15′ at 4 °C. The supernatants containing proteins extract were collected. Nuclear and cytoplasmic fractionation was performed by a modification of the method described previously [29]. Briefly, cells were trypsinized and washed twice in ice-cold PBS and lysed on ice for 15 min in cytoplasmic lysis buffer (10 mM HEPES, pH 7.9, 50 mM NaCl, 0.5 M Sucrose, 0.1 mM EDTA, 0.5% Tryton, 1 mM dithiothreitol, 1 mM Na_2 VO_4, 1 mM Sodium Fluoride, 0.5 mM Phenylmethanesulfonyl fluoride, Protease Inhibitor Cocktail, 17.5 mM β-glycerophosphate, all from Sigma). Nuclei were pelleted by centrifugation (2000 rpm, 10′ at 4 °C), and the supernatant, containing the cytoplasmic/membrane extract, cleared centrifuging at 14,000 rpm, 15′ at 4 °C.

Nuclear pellet was washed by centrifugation, at 2000 rpm for 10′ at 4 °C, in 10 mM HEPES, pH 7.9, 10 mM KCl, 0.1 mM EDTA, 0.1 mM EGTA, 1 mM Na_2 VO_4, 1 mM Sodium Fluoride, 0.5 mM Phenylmethanesulfonyl fluoride, Protease Inhibitor Cocktail (all from Sigma). Nuclei were lysed by vortexing for 30 min at 4 °C in nuclei lysis buffer (10 mM HEPES, pH 7.9, 500 mM NaCl, 0.1 mM EDTA, 0.1 mM EGTA, 0.1% IGEPAL, 1 mM Na_2 VO_4, 1 mM Sodium Fluoride, 0.5 mM Phenylmethanesulfonyl fluoride, Protease Inhibitor Cocktail, all from Sigma) and centrifuged at 14,000 rpm, 10′ at 4 °C. The supernatant, containing the nuclear extract, was collected. Protein concentration of cytoplasmic and nuclear extracts was measured by BCA protein assay (Biorad). For Western blotting, 30 μg of proteins were separated by SDS-PAGE, transferred and immobilized on a nitrocellulose membrane 0.45 μm (Amersham). Membranes were blocked for 1 h at room temperature, with 5% non fat milk or 5% Bovine Serum Albumin in TBS (Tris–HCl 50 mM, pH 7.4, NaCl 150 mM) containing 0.2% Tween 20 and hybridized overnight at 4 °C, with either: rabbit polyclonal to TFEB (Abcam, ab96834; 1:500), mouse monoclonal to LAMP2 (Abcam, ab25631; 1:250), rabbit polyclonal to Fibrillarin (Abcam, ab5821; 1:1000), and rabbit polyclonal to Actin (Sigma, a2066; 1:2000). Primary antibodies were detected using horseradish peroxidase-linked anti-mouse or anti-rabbit secondary antibodies (DAKO, Cambridge, UK) and visualized using the enhanced chemiluminescent detection system (SuperSignal West Dura Extended Duration Substrate, Thermo Scientific).

2.8. Statistics

Characteristics of the study population are described using mean ± standard deviation while results regarding CSC assays are shown as median, 10th and 90th percentile. Data were analyzed for normal distribution by Kolmogorov–Smirnov test. Fisher's exact test was used to compare proportions. Two-tailed unpaired t-test or Mann–Whitney test, as appropriate, was used to compare continuous variables between two independent groups. Drug-treatment assays were analyzed by two-tailed paired t-test or Wilcokson matched pairs test, as appropriate. Probability values (p) less than 0.05 were considered significant. Analyses were conducted with Prism, version 4.0c and SPSS20 for Macintosh software.

3. Results

3.1. E-CSC transcriptome is deficient in lysosomal network mRNAs

With the aim to identify transcriptomic imbalances associated with the lysosomal network, the CSC's transcriptional profiles data, showed in [2], were integrated with a new pair of D- and E-CSC and analyzed according to the last version of gene annotation (http://www.ncbi.nlm.nih.gov/gene). This study enabled the identification of genes differentially expressed between the two classes of CSC (B.H $p < 0.05$; supplementary Table S2) To understand the biological meaning of the transcriptomic analysis results, the functional annotations of differently expressed gene lists were examined with Ingenuity Pathway analysis (IPA). Both up- and down-regulated identifiers were defined as value parameters for the analysis. After the analysis, generated biological functions and the canonical pathways were ordered by the statically significance score ($-\log.p$-value). In this case biological pathways that were related to the term "lysosome" were very significant. In fact the most enriched canonical pathway overall was "Caveolar-mediated Endocytosis Signaling" and other elements, such as "phagosome maturation and formation" and "Clathrin-mediated Endocytosis Signaling", were strongly enriched (Fig. 1A and supplementary Table S3). We obtained similar results in the KEGG pathway analysis using Clusterprofiler tool (Table S4). At the gene level, genes associated with lysosomal pathways (ADA, CTSK, CTSL, DAB2, FNBP1, MLC1, TMEM9, DPP7, LUM, ASAH1, OCA2, CTSA, WDR48, TCN2, GPR137B, USP5, CAT) were down regulated in the transcriptome of E-CSC (Fig. 1B). We then created a Lysosome gene set (Table S5, n = 170) performing an automated literature search using IPA and we confirmed the statistical association between the transcriptional program of E-CSC and this gene set (Fisher's exact test, $p < 0.005$). Intriguingly, other pathways that are predicted as inactivated and are related with cardiac pathology were "Role of NFAT in Cardiac Hypertrophy", "Protein Kinase A Signaling" and "Cardiac Hypertrophy

Table 2
LIST of 29 genes, direct target of TFEB, that are down-regulated in E-CSC.

Gene symbol	Entrez GeneId	Gene name
ATP6V1B2	526	ATPase, H+ transporting, lysosomal 56/58 kDa, V1 subunit B2
BSG	682	Basigin (Ok blood group)
CAMKK1	84254	Calcium/calmodulin-dependent protein kinase kinase 1, alpha
CHAF1A	10036	Chromatin assembly factor 1, subunit A (p150)
CLCN7	1186	Chloride channel, voltage-sensitive 7
DIP2B	57609	DIP2 disco-interacting protein 2 homolog B (Drosophila)
DLX2	1746	Distal-less homeobox 2
DPP7	29952	Dipeptidyl-peptidase 7
EEF1A1	1915	Eukaryotic translation elongation factor 1 alpha 1
GSTO1	9446	Glutathione S-transferase omega 1
KCNAB2	8514	Potassium voltage-gated channel, shaker-related subfamily, beta member 2
LZTS2	84445	Leucine zipper, putative tumor suppressor 2
MAX	4149	MYC associated factor X
NAGLU	4669	N-acetylglucosaminidase, alpha
PLD3	23646	Phospholipase D family, member 3
RAD23A	5886	RAD23 homolog A (*S. cerevisiae*)
RNF146	81847	Ring finger protein 146
RNF185	91445	Ring finger protein 185
SDF4	51150	Stromal cell derived factor 4
SLC31A2	1318	Solute carrier family 31 (copper transporter), member 2
SSR3	6747	Signal sequence receptor, gamma (translocon-associated protein gamma)
TACC2	10579	Transforming, acidic coiled-coil containing protein 2
TAGLN2	8407	Transgelin 2
TBK1	29110	TANK-binding kinase 1
TMEM8A	58986	Transmembrane protein 8A
UBA52	7311	Ubiquitin A-52 residue ribosomal protein fusion product 1
UBE4B	10277	Ubiquitination factor E4B
WDR45	11152	WD repeat domain 45
ZC3H11A	9877	Zinc finger CCCH-type containing 11A

Summary of the 29 genes that are target of TFEB whose expression is down regulated in E-CSC.

Signaling". At the same time "PPARα/RXRα Activation", "TWEAK signaling" and "TNFR1 signaling" were activated (see Table S3).

Since growing evidences report that Transcription Factor EB (TFEB) plays an integrated control of cellular clearance pathways regulating the transcription of a set of genes known as CLEAR gene network, the presence of validated targets of TFEB [11] was evaluated among the E-CSC down-regulated genes. This investigation revealed 29 genes, less expressed in E-CSC, that are part of the CLEAR network (Table 2).

Altogether, these results indicate that CSC obtained from failing hearts were characterized by an altered regulation of a gene set involved in cellular clearance processes linked with lysosomes.

3.2. The function of the E-CSC's Lysosomal Compartment is weakened

In order to evaluate the function of CSC's lysosomes, we first assessed the pH of these organelles by employing both a fluorescent pH indicator (i.e. the LysoSensor Blue DND-167 that is almost non-fluorescent except when inside acidic compartments) and Acridine Orange – AO – (i.e. a metachromatic dye that displays a red fluorescence in acidic lysosomes, while it shifts towards green as a consequence of a rise of lysosome pH) [30]. Confocal analysis of Lysosensor vital staining showed that the blue fluorescence of D-CSC was more than five-fold more intense than the E-CSC one (Fig. 2A–C). These data were further corroborated quantitating the red emission of AO by flow cytometry (Fig. 2D, E).

In order to exclude that the observed difference in the fluorescence intensity of lysosomes was due to a difference in the lysosomal mass, we analyzed CSC employing both LysoTracker Red DND-99 vital staining and Western Blotting (WB) for Lysosomal Associated Membrane Protein 2 (LAMP2). Neither flow-cytometry (Fig. 3C, D) nor WB analyses (Fig. 3E, F) showed significant differences in terms of LC size.

Signs of an altered lysosomal function were studied in depth by evaluating: the presence of both intra-lysosomal lipofuscins, the activity of Cathepsin B, and evidence of lysosomal membrane permeabilization, such as the formation of Galectin 3 *punctae* [31]. To this aim, we first documented, by spectral analysis performed through confocal microscopy, the presence of autofluorescent intracellular inclusions showing the typical emission spectrum of lipofuscins (that peaks at 580–600 nm [32], Fig. 4). Moreover, we demonstrated that this pigment is significantly more abundant in the lysosomes of E-CSC (Fig. 5A–C). Subsequently, we demonstrated that, with respect to D-CSC, E-CSC are characterized by: a significantly reduction of Cathepsin B activity, as evaluated employing a vital fluorescent assay (Fig. 5D–F), and a significant increase in the proportion of cells with lysosomal permeabilization, as assessed by the presence of Galectin 3 *punctae* localized to lysosomes. (Fig. 5G–I).

Since eukaryotic cells rely on the master regulator Transcription Factor EB to promote the clearance of lysosomes [7], the activation status of TFEB was evaluated. Confocal microscopy and WB analyses demonstrated that the amount of nuclear activated TFEB is significantly higher in D-CSC with respect to E-CSC (Fig. 6).

Altogether these results suggest that CSC isolated from failing explanted hearts are characterized by a compromised LC and, as a consequence, by reduced digestive potential.

3.3. mTORC1 inhibition restores the function of E-CSC's Lysosomal Compartment

Next, we investigated whether a pharmacological treatment was able to counteract the described lysosomal network impairments. With this intent, Rapamycin was employed because of its recently reported effectiveness in contrasting senescence, reactivating E-CSC's autophagic flux by reducing mTORC1 hyperactivation [3]. Specifically the same drug treatment conditions used in [3] were followed. A three-day treatment with 10 nM Rapamycin was able to potentiate the LC functionality, as suggested by the significant increase of both lysosomal acidity (Fig. 7A–C), and Cathepsin B activity (Fig. 7D–F). Drug treatment was additionally associated with a trend towards increased levels of LAMP2 (Fig. 7 **G,H**). Moreover, data obtained from confocal images demonstrated that the single dose therapy was able to downsize the mass of lipofuscin (Fig. 7I–K) as well as the fraction of cells characterized by Galectin-3 *punctae* (Fig. 7L–N).

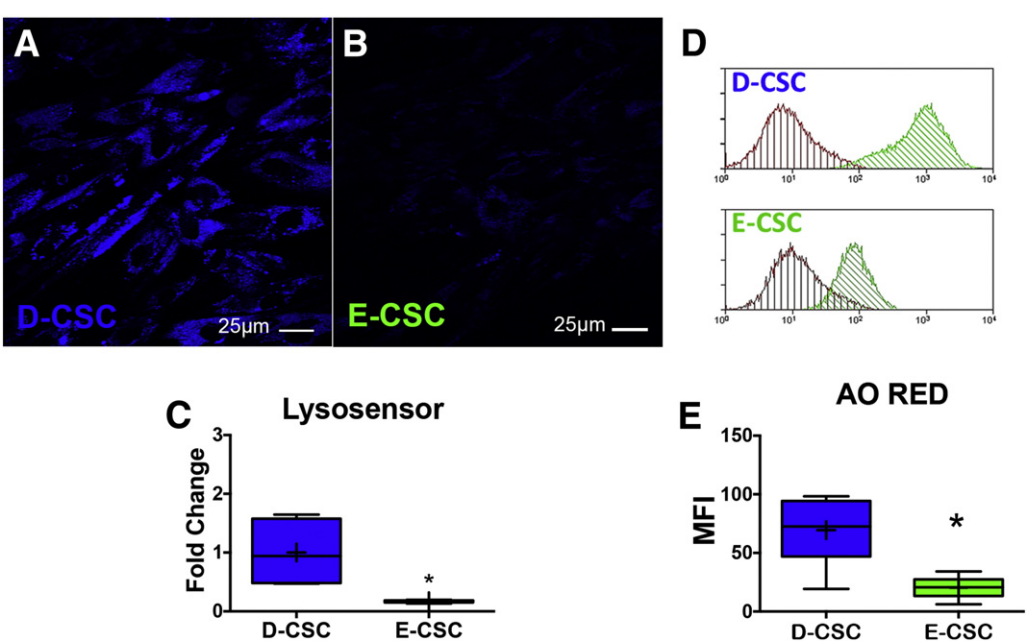

Fig. 2. Lysosomal Functionality Assay in CSC. Representative confocal images of cultured D-CSC (A) and E-CSC (B) stained by the fluorescent vital pH indicator LysoSensor Blue DND-167. Bar graph in C displays the fold change in the Integrated Fluorescence Intensity (IFI) of E-CSC (n = 5) with respect to D-CSC (n = 5). D: representative Flow-Cytometry histograms of cultured D- (n = 7) and E-CSC (n = 5) analyzed after incubation with Acridine Orange (AO). The red florescence emission of AO stained cells is reported by green histograms that are superimposed with control profiles of unstained cells (red histograms). Bar graph in E summarizes quantitative Flow-Cytometry results that are expressed as Mean Fluorescence Intensity (MFI) of red emission from cells stained with AO. In bar graphs (C, E) data are presented as median, 10th and 90th percentile, crosses indicate means. * $p < 0.05$ vs D-CSC.

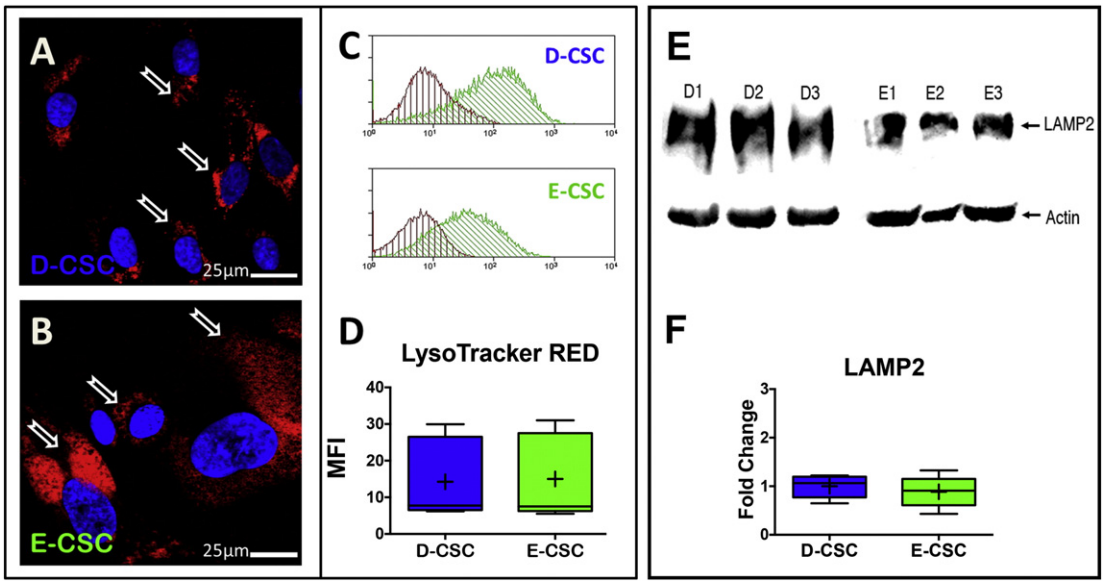

Fig. 3. Evaluation of Lysosomal Compartment Size in CSC. Representative confocal images of D-CSC (A) and E-CSC (B) lysosomes, stained by LysoTracker Red DND-99 (red) and pointed out by arrows. Nuclei are shown by the blue fluorescence of DAPI. C: representative Flow-Cytometry histograms of cultured D- (n = 7) and E-CSC (n = 5) analyzed after incubation with LysoTracker Red DND-99. The red florescence emission of stained cells is reported by green histograms that are superimposed with control profiles of unstained cells (red histograms). Plots in D summarize quantitative Flow-Cytometry results that are expressed as Mean Fluorescence Intensity (MFI) of red emission from cells stained with LysoTracker Red DND-99. Data are presented as median, 10th and 90th percentile, crosses indicate means. E: Representative Western blots of cell extracts obtained from three D-CSC (D1, D2 and D3) and three E-CSC (E1, E2 and E3). Blotted proteins were incubated with antibodies directed against LAMP2 and actin. Histograms in F show the results of the densitometric analyses (n = 5 D- and 5 E-CSC) expressed as fold change with respect to D-CSC. Data are presented as median, 10th and 90th percentile, crosses indicate means. $^{*}p < 0.05$ vs D-CSC.

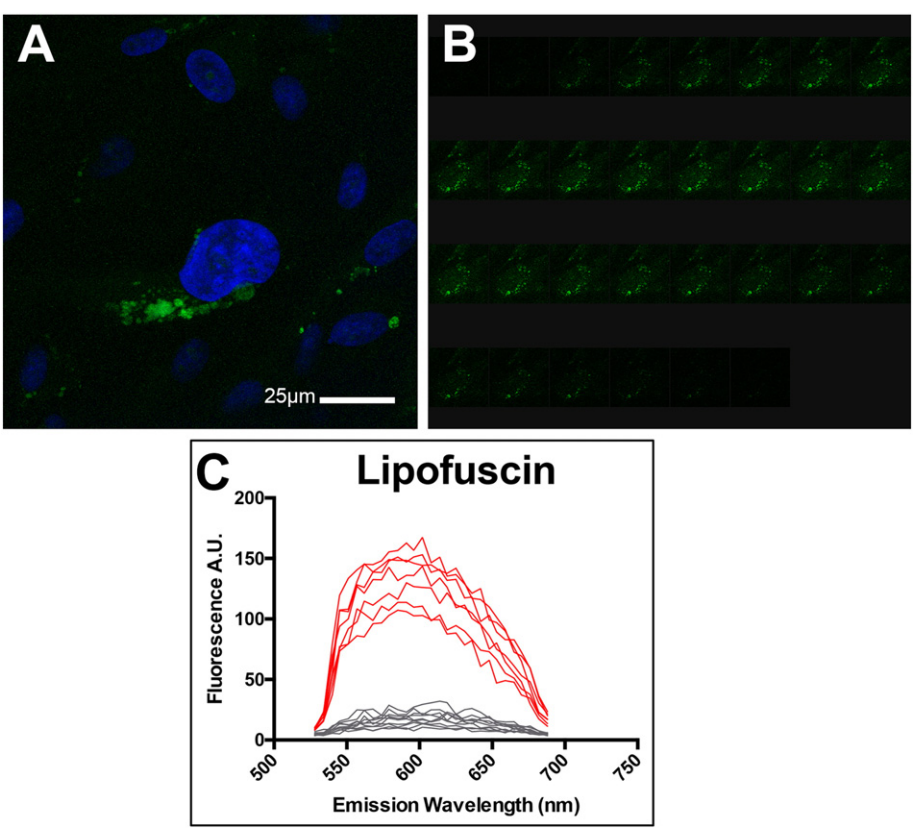

Fig. 4. Spectral analysis of Lipofuscin. Confocal images showing the accumulation of autofluorescent intracellular granules in E-CSC (A). Nuclei are shown by the blue fluorescence of DAPI. Autofluorescence emission spectra of lipofuscins were evaluated performing a λ-scanning by confocal microscopy, exciting unstained cells at $\lambda = 514$ nm and collecting emitted fluorescence, between 528 nm and 688 nm, every $\approx$5 nm (B). Fluorescence emission spectra, evaluated both in autofluorescent (red lines) and non-autofluorescent cells (gray lines), showed a typical emission peak at about 580–600 nm (C).

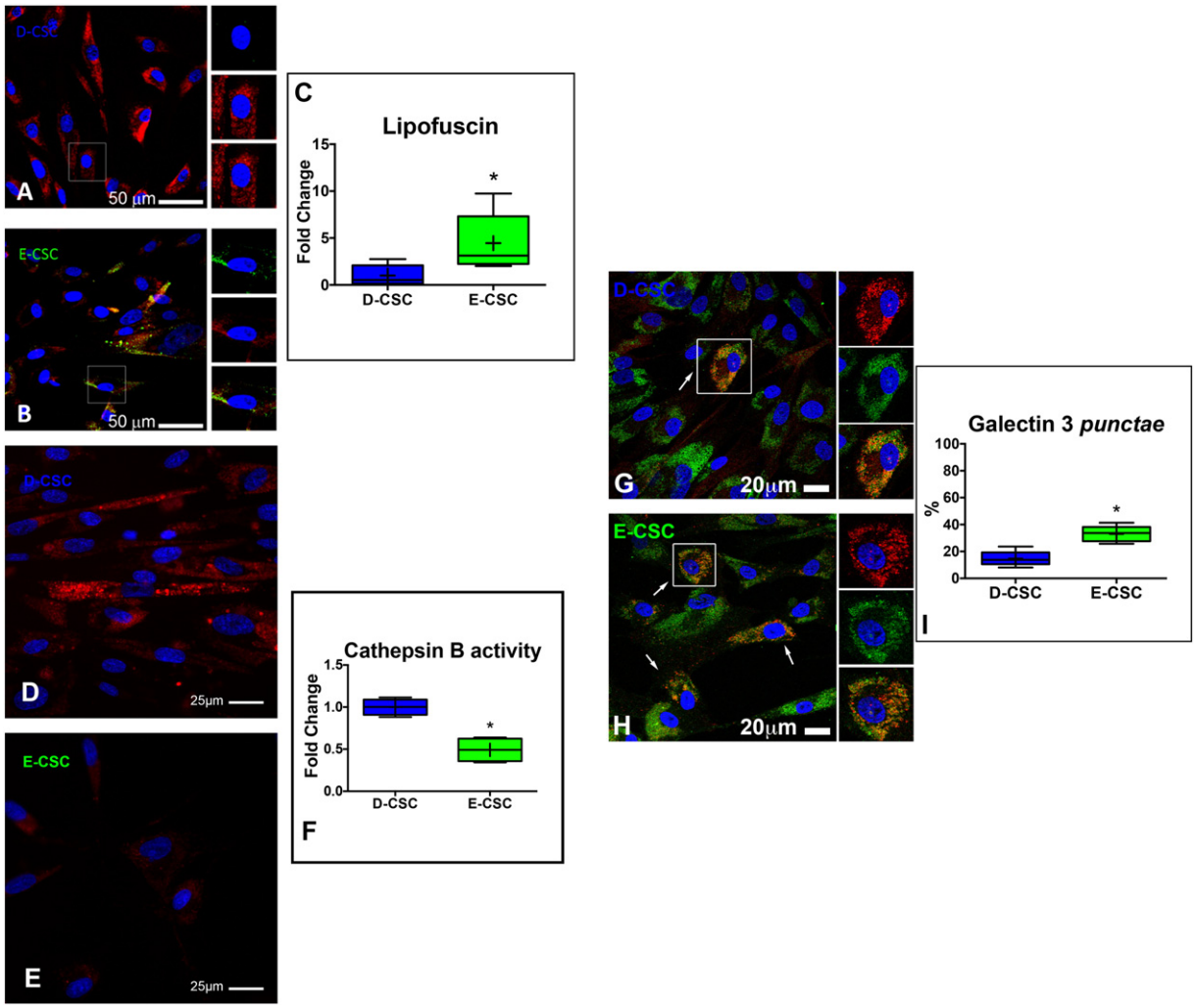

Fig. 5. Lysosomal Level of Lipofuscin, Cathepsin B activity and presence of Galectin 3 *punctae* in CSC. (A–C) Lipofuscins. Representative confocal images of cultured D-CSC (A) and E-CSC (B) illustrating colocalization of lysosomes (marked by LAMP-2, red) with autofluorescent lipofuscins (green). Nuclei are shown by the blue fluorescence of DAPI. Split channel images of the cells comprised in the squares are shown at a higher magnification in the right portion of each figure. The histogram in C summarizes the fold change in the lipofuscin IFI in the Lysosomal Compartment of E-CSC (n = 5) with respect to D-CSC (n = 5). Data are presented as median, 10th and 90th percentile, crosses indicate means. $^{*}p < 0.05$ vs D-CSC. (D–F) Cathepsin B activity. Representative epifluorescence images of cultured D-CSC (D) and E-CSC (E) displaying the presence of a red fluorescent product expression of Cathepsin B activity. Nuclei are depicted by the blue fluorescence of DAPI. The bar graphs in F display the fold change in cathepsin B activity of E-CSC (n = 4) with respect to D-CSC (n = 4). Data are presented as median, 10th and 90th percentile, crosses indicate means. $^{*}p < 0.05$ vs D-CSC. (G–I) Galectin *punctae*. Representative confocal images of cultured D-CSC (G) and E-CSC (H) illustrating galectin 3 positivity (red fluorescence). Cells displaying galectin 3 *punctae* are indicated by arrows. Nuclei are shown by the blue fluorescence of DAPI. Split channel images of the cells comprised in the squares are shown at a higher magnification in the right portion of each figure to display colocalization of lysosomes (marked by LAMP-2, green) with galectin 3. The histogram in I summarizes the fraction of CSC presenting galectin 3 *punctae*. Data are presented as median, 10th and 90th percentile, crosses indicate means. $^{*}p < 0.05$ vs D-CSC.

Last, quantitative measurement of nuclear Trascription Factor EB proved that the active form of TFEB was significantly higher in drug-treated E-CSC compared to Vehicle-treated ones (Fig. 7O–Q).

Altogether these results suggested that the conditioning of E-CSC for three days with 10 nM Rapamycin is effective in reversing their dysfunctional LC, thereby ameliorating their degradative potential.

4. Discussion

We have previously showed that, in CSC cultured from failing hearts (E-CSC), cell senescence is paralleled by a block in autophagic activity. Here, we newly investigated the causes of this autophagic flux arrest by comparing the status of the lysosomal network in CSC obtained from normal hearts (D-CSC) with that of E-CSC.

Bioinformatics analysis on the functional meaning of differentially expressed genes underlined that CSC obtained from normal and pathologic hearts are involved in: lysosomal related, junction related, cytokine/external signaling related, signal transduction related and transcription factor related biological themes. These data support the notion that the milieu (i.e. that of a failing heart) conditions their gene expression profile, possibly by epigenetic alterations. In line with our data, a recent work by Vecellio and colleagues demonstrates that cardiac derived mesenchymal stem cells isolated from diabetic hearts retain an epigenetic memory of their diseased organ of origin [33]. Interestingly, the expression of a subset of genes implicated in protein degradation bypassing lysosomes are more expressed in E-CSC, suggesting that a plausible compensatory mechanism is made necessary by an inadequate lysosomal digestion. This latter is supported by the fact that genes encoding for proteins, that are attributable to the structure of lysosomes and other lytic vacuoles, or associated to the proteolysis process are down-regulated in explanted cells. To complete the framework, the involvement of Transcription Factor EB (TFEB) was considered, given its centrality in controlling cellular clearance pathways, promoting the transcription of a set of genes known as CLEAR (Coordinated Lysosomal Expression and Regulation) gene network [10,13]. The present work newly discovered 29 TFEB direct target genes that are less expressed

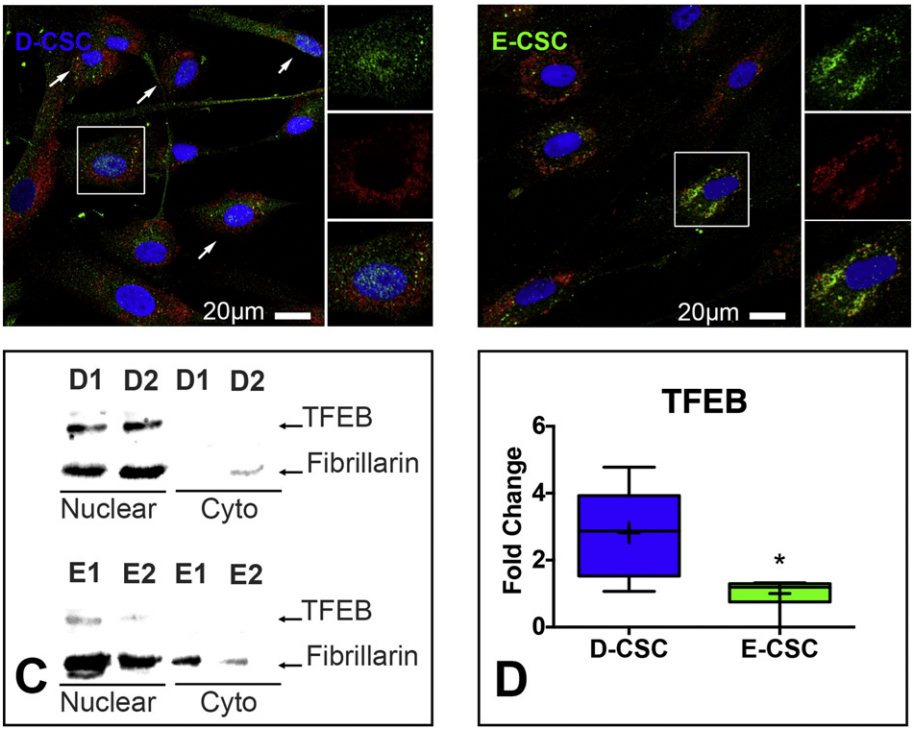

Fig. 6. Evaluation of Active Nuclear TFEB on CSC. Representative confocal images of cultured D-CSC (A), and E-CSC (B), after immunostaining with antibodies against TFEB (green), and LAMP-2 (red). Nuclei are shown by the blue fluorescence of DAPI. Split channel images of the cells comprised in the squares are shown at a higher magnification in the right portion of each figure. C: Representative Western blots of nuclear and cytoplasmic cell extracts obtained from two D-CSC (D1 and D2) and two E-CSC (E1 and E2). Blotted proteins were incubated with antibodies directed against TFEB and the nucleolar protein fibrillarin. Histograms in D show the results of the quantitation of the IFI of TFEB within the nuclei of D-CSC ($n = 6$) and E-CSC ($n = 6$). Data are presented as median, 10th and 90th percentile, crosses indicate means. $^{*}p < 0.05$ vs D-CSC.

in failing heart derived-CSC, suggesting that TFEB is less active in E-CSC than in D-CSC. The reduced activity of this transcription factor may, in fact, account for the diminished transcription of lysosomal network genes [14].

The newly recognized transcriptome imbalances associated with E-CSC's Lysosomal Compartment (LC) drove our research towards the direct examination of lysosomal size and functionality. Interestingly, our analyses, although excluding differences in terms of LC extension, reported that lysosomes of CSC obtained from end-stage failing hearts are less acidic and less functional. In order to corroborate this finding, we evaluated the activity of Cathepsin B, and showed that it is depressed in patient-derived CSC. Although the involvement of cathepsins in cardiovascular disease is complex, cathepsin B has been shown to be upregulated following myocardial infarction. Moreover, inhibition of cathepsin B activity has been coupled with fibrosis [34].To further validate these functional differences in the LC, we assessed the amount of undigested material, known as lipofuscin, that was accumulated within the lysosomes, jeopardizing their digestive capability, and their fusion with the autophagosomes [20]. Quantitatively, we showed that the load of lipofuscin is more than 5-fold higher in lysosomes of E-CSC. Furthermore we demonstrated that explanted CSC express also higher level of lysosomal-localized Galectin 3 (Gal-3). This latter is a lectin with high affinity for ß-galactosides, that is distributed throughout both the cytoplasm and the nucleus. ß-galactose-containing glycoproteins are localized only on the cell surface and in the lumen of endocytic compartments, therefore they interact with Gal-3 only as a result of endosomal membrane rupture. Recent data have demonstrated that a re-localization of Gal-3 from the cytoplasm to the Lysosomal Compartment (i.e. formation of galectin *punctae*) occurs as a consequence of lysosome membrane permeabilization, therefore its quantitation has been considered a very sensitive assay to study the status of lysosomes [35].

Moving from the above-described observations, the activation of TFEB was investigated. This latter, in fact, promotes the clearance of lysosomes, favoring their fusion with plasma membrane, in order to remove their toxic content by exocytosis [7]. Consistently with gene expression profile data, we demonstrated that the amount of nuclear active TFEB is significantly lower in E-CSC, that are consequently less effective in cutting out their dysfunctional lysosomes.

Our subsequent aim was, therefore, to develop a drug-based strategy able to reverse the above-described alterations and boost LC functionality. Given its ability to unblock E-CSC's autophagic flux by inhibiting the TORC1 superactivation [3], the drug chosen for the E-CSC treatment was Rapamycin. The effectiveness of our strategy in restoring the LC function of explanted cells was underlined by: the restoration of the acidity of lysosomes, the increase of cathepsin-B activity, the decreased load of lipofuscin in lysosomes, and the restored nuclear localization of TFEB. These results are in line with recent data obtained by Settembre and colleagues, who demonstrated that mTORC1 inactivates TFEB by a transient interaction on lysosomal membrane [14].

Therefore TFEB, senescence, and mTORC1 may play the roles of *the Good*, *the Bad* and *the Ugly*, respectively. Specifically, chronic stress and inflammatory conditions, to which CSC resident in failing hearts have to respond, push the cells towards a senescent phenotype, that is characterized by a hyperactivation of mTORC1 [3]. This latter, in addition to directly inhibit autophagy, also prevents the nuclear translocation of TFEB, thus switching off its ability to orchestrate and promote the degradation activity of the cell. As a consequence, both the biogenesis of new lysosomes and the disposal of toxic substances by lysosomal exocytosis are impaired. Because of this, waste materials accumulate

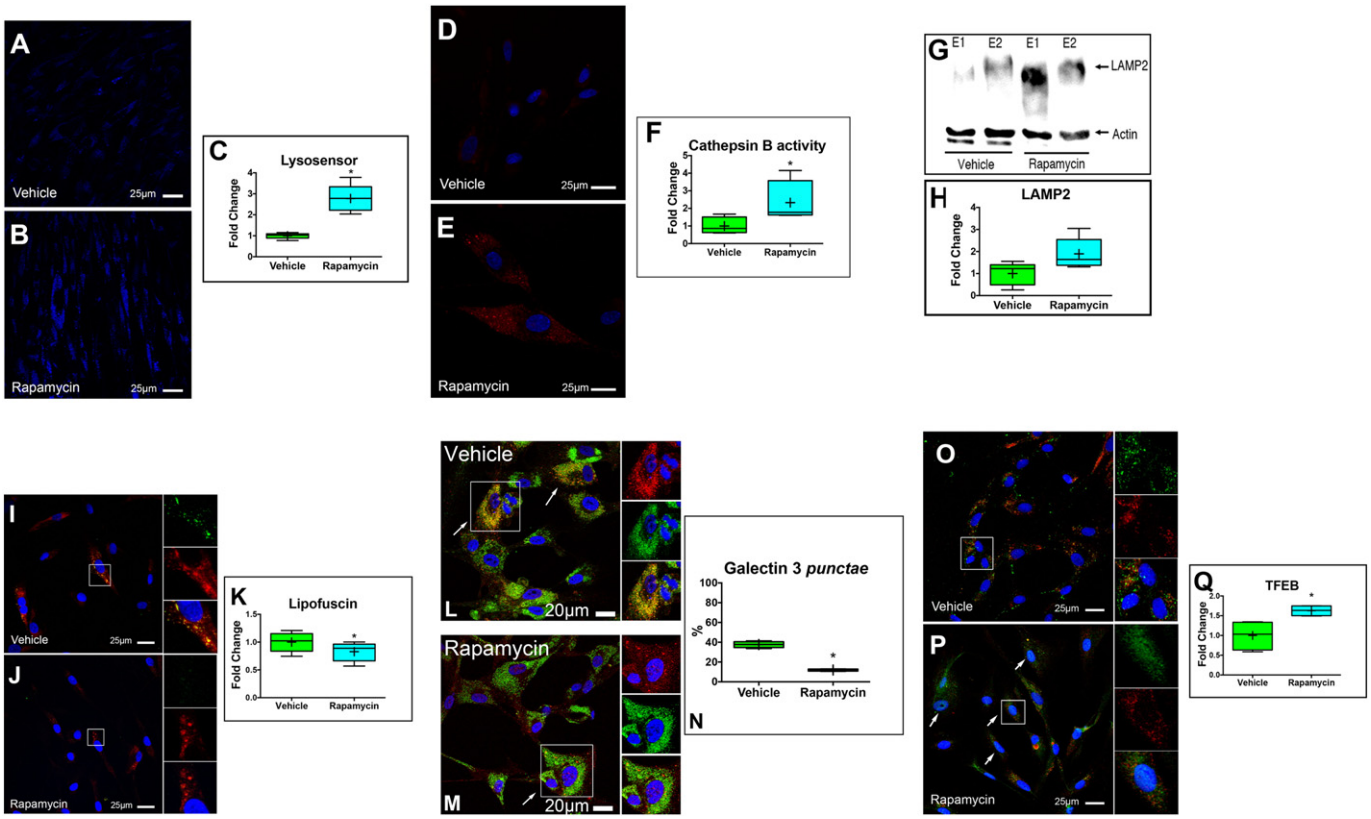

Fig. 7. Effects of Rapamycin Treatment of E-CSC on Lysosome Size and Functionality. (A–C) Lysosome acidity. Representative confocal images of E-CSC treated with Vehicle (A) or Rapamycin (B) and stained by the fluorescent vital pH indicator LysoSensor Blue DND-167. Bar graph in C displays the fold change in the Mean Fluorescence Intensity (MFI) of Rapamycin-treated E-CSC (n = 5) with respect to those vehicle-treated (n = 5). Data are presented as median, 10th and 90th percentile, crosses indicate means. $^{*}p < 0.05$ vs D-CSC. (D–F) Cathepsin B activity. Representative epifluorescence images of cultured E-CSC treated with Vehicle (D) or Rapamycin (E) displaying the presence of a red fluorescent product expression of Cathepsin B activity. Nuclei are depicted by the blue fluorescence of DAPI. The bar graphs in F display the fold change in cathepsin B activity of Rapamycin-treated E-CSC (n = 4) with respect to those Vehicle-treated (n = 4). Data are presented as median, 10th and 90th percentile, crosses indicate means. $^{*}p < 0.05$ vs D-CSC. (G–H) LAMP2 expression. Representative Western blots of cell extracts obtained from two E-CSC (E1 and E2) treated either with vehicle or Rapamycin. Blotted proteins were incubated with antibodies directed against LAMP2 and actin (G). Histograms in H show the results of the densitometric analyses expressed as fold change in LAMP2 levels of Rapamyicin treated E-CSC (n = 5) with respect to the Vehicle-treated ones (n = 5). Data are presented as median, 10th and 90th percentile, crosses indicate means. $^{*}p < 0.05$ vs D-CSC. (I–K) Lipofuscins. Representative confocal images of cultured E-CSC treated with Vehicle (I) or Rapamycin (J) illustrating the co-localization of lysosomes (marked by LAMP-2, red) with autofluorescent lipofuscins (green). Nuclei are shown by the blue fluorescence of DAPI. Split channel images of the cells comprised in the squares are shown at a higher magnification in the right portion of each figure. The histogram in K summarizes the fold change in the lipofuscin IFI in the Lysosomal Compartment of Rapamycin-treated E-CSC (n = 5) with respect to those vehicle-treated (n = 5). Data are presented as median, 10th and 90th percentile, crosses indicate means. $^{*}p < 0.05$ vs D-CSC. (L–N) Galectin *punctae*. Representative confocal images of E-CSC treated with Vehicle (L) or Rapamycin (M) illustrating colocalization of lysosomes (marked by LAMP-2, green) with galectin 3 (red fluorescence). Cells displaying galectin 3 *punctae* are indicated by arrows. Nuclei are shown by the blue fluorescence of DAPI. Split channel images of the cells comprised in the squares are shown at a higher magnification in the right portion of each figure. The histogram in N summarizes the fraction of E-CSC presenting galectin 3 *punctae* in Rapamycin- (n = 5) vs. Vehicle-treated cells (n = 5). Data are presented as median, 10th and 90th percentile, crosses indicate means. $^{*}p < 0.05$ vs D-CSC. (O–Q) Active Nuclear TFEB. Representative confocal images of E-CSC treated with Vehicle (O) or Rapamycin (P), after immunostaining with antibodies against TFEB (green), and LAMP-2 (red). Nuclei are shown by the blue fluorescence of DAPI. Split channel images of the cells comprised in the squares are shown at a higher magnification in the right portion of each figure. The bar graph in Q summarizes the fold change of the IFI of nuclear TFEB in Rapamycin- (n = 4) vs. Vehicle-treated cells (n = 4). Data are presented as median, 10th and 90th percentile, crosses indicate means. $^{*}p < 0.05$ vs D-CSC.

within the lysosome, generating lipofuscin that jeopardize its digestive potential and inhibit its fusion with autophagosomes. As a result, the autophagy-lysosome pathway and the cellular clearance mechanisms decline, thus threatening protein homeostasis, and leading to new stress, inflammatory conditions and, as a consequence, to cell senescence and aging [36]. Noteworthy, Rapamycin treatment interrupts upstream this vicious cycle by inhibiting mTORC1 and is effective in restoring E-CSC's LC functionality, awakening the digestive potential of these cells.

In conclusion, we show, in the present work, the central role played by the lysosome in altering the biological properties of CSC, and in dictating their complex senescent phenotype.

Supplementary data to this article can be found online at http://dx.doi.org/10.1016/j.ijcard.2016.04.155.

Competing interests

Nothing to declare.

Acknowledgments

We thank prof. Ballabio (Telethon Institute of Genetics and Medicine, TIGEM; Naples, Italy) for the list of TFEB direct gene targets. We wish to thank Molino Moras for supporting the PhD program of G.G. A.C. is supported by a fellowship provided by Beneficentia Stiftung. Y. C. is supported by the AIRC/FIRC fellowship.

References

[1] C. Lopez-Otin, M.A. Blasco, L. Partridge, et al., The hallmarks of aging. [research support, non-U.S. Gov't review], Cell 153 (6) (2013) 1194–1217.

[2] D. Cesselli, A.P. Beltrami, F. D'Aurizio, et al., Effects of age and heart failure on human cardiac stem cell function, Am. J. Pathol. 179 (1) (2011) 349–366.

[3] E. Avolio, G. Gianfranceschi, D. Cesselli, et al., Ex vivo molecular rejuvenation improves the therapeutic activity of senescent human cardiac stem cells in a mouse model of myocardial infarction, Stem Cells 32 (9) (2014) 2373–2385.

[4] Y.S. Rajawat, Z. Hilioti, I. Bossis, Aging: central role for autophagy and the lysosomal degradative system, Ageing Res. Rev. 8 (3) (2009) 199–213.
[5] K.C. Jefferies, D.J. Cipriano, M. Forgac, Function, structure and regulation of the vacuolar (H+)-ATPases, Arch. Biochem. Biophys. 476 (1) (2008) 33–42.
[6] P. Boya, G. Kroemer, Lysosomal membrane permeabilization in cell death, Oncogene 27 (50) (2008) 6434–6451.
[7] L. Medina Diego, A. Fraldi, V. Bouche, et al., Transcriptional activation of lysosomal exocytosis promotes cellular clearance, Dev. Cell 21 (3) (2011) 421–430.
[8] W. Ge, D. Li, Y. Gao, et al., The roles of lysosomes in inflammation and autoimmune diseases, Int. Rev. Immunol. (2014).
[9] H. Appelqvist, P. Waster, K. Kagedal, et al., The lysosome: from waste bag to potential therapeutic target, J. Mol. Cell Biol. 5 (4) (2013) 214–226.
[10] M. Sardiello, M. Palmieri, A. di Ronza, et al., A gene network regulating lysosomal biogenesis and function, Science 325 (5939) (2009) 473–477.
[11] M. Palmieri, S. Impey, H. Kang, et al., Characterization of the CLEAR network reveals an integrated control of cellular clearance pathways, Hum. Mol. Genet. 20 (19) (2011) 3852–3866.
[12] C. Settembre, C. Di Malta, V.A. Polito, et al., TFEB links autophagy to lysosomal biogenesis, Science 332 (6036) (2011) 1429–1433.
[13] C. Settembre, A. Ballabio, TFEB regulates autophagy: an integrated coordination of cellular degradation and recycling processes, Autophagy 7 (11) (2011) 1379–1381.
[14] C. Settembre, R. Zoncu, D.L. Medina, et al., A lysosome-to-nucleus signalling mechanism senses and regulates the lysosome via mTOR and TFEB, EMBO J. 31 (5) (2012) 1095–1108.
[15] G. Gianfranceschi, G. Gri, D. Cesselli, et al., Stem cell senescence as the memory of past injuries, Curr. Pathobiol. Rep. 3 (1) (2015) 17–26.
[16] A. Terman, U.T. Brunk, Is aging the price for memory? Biogerontology 6 (3) (2005) 205–210.
[17] A. Ulbricht, V. Arndt, J. Hohfeld, Chaperone-assisted proteostasis is essential for mechanotransduction in mammalian cells, Commun. Integr. Biol. 6 (4) (2013) e24925.
[18] A.P. Beltrami, D. Cesselli, C.A. Beltrami, Stem cell senescence and regenerative paradigms, Clin. Pharmacol. Ther. 91 (1) (2012) 21–29.
[19] C. Chimenti, J. Kajstura, D. Torella, et al., Senescence and death of primitive cells and myocytes lead to premature cardiac aging and heart failure, Circ. Res. 93 (7) (2003) 604–613.
[20] B. Levine, G. Kroemer, Autophagy in the pathogenesis of disease, Cell 132 (1) (2008) 27–42.
[21] A. Terman, T. Kurz, B. Gustafsson, et al., The involvement of lysosomes in myocardial aging and disease, Curr. Cardiol. Rev. 4 (2) (2008) 107–115.
[22] A.P. Beltrami, D. Cesselli, N. Bergamin, et al., Multipotent cells can be generated in vitro from several adult human organs (heart, liver, and bone marrow), Blood 110 (9) (2007) 3438–3446.
[23] D. Cesselli, F. D'Aurizio, P. Marcon, et al., Cardiac stem cell senescence, Methods Mol. Biol. 976 (2013) 81–97.
[24] G. Yu, L.-G. Wang, Y. Han, et al., clusterProfiler: an R package for comparing biological themes among gene clusters, OMICS 16 (5) (2012) 284–287.
[25] The Gene Ontology C, M. Ashburner, C.A. Ball, et al., Gene ontology: tool for the unification of biology, Nat. Genet. 25 (1) (2000) 25–29.
[26] M. Kanehisa, S. Goto, M. Furumichi, et al., KEGG for representation and analysis of molecular networks involving diseases and drugs, Nucleic Acids Res. 38 (Database issue) (2010) D355–D360.
[27] W. Luo, C. Brouwer, Pathview: an R/Bioconductor package for pathway-based data integration and visualization, Bioinformatics 29 (14) (2013) 1830–1831.
[28] C.A. Schneider, W.S. Rasband, K.W. Eliceiri, NIH image to ImageJ: 25 years of image analysis, Nat. Methods 9 (7) (2012) 671–675.
[29] H.P. Harding, Y. Zhang, D. Ron, Protein translation and folding are coupled by an endoplasmic-reticulum-resident kinase, Nature 397 (6716) (1999) 271–274.
[30] M. Olsson, I. Rundquist, U. Brunk, Flow cytofluorometry of lysosomal acridine orange uptake by living cultured cells effect of trypsinization and starvation, Acta Pathol. Microbiol. Scand. A Pathol. 95A (1–6) (1987) 159–165.
[31] I. Paz, M. Sachse, N. Dupont, et al., Galectin-3, a marker for vacuole lysis by invasive pathogens, Cell. Microbiol. 12 (4) (2010) 530–544.
[32] D. Yin, Biochemical basis of lipofuscin, ceroid, and age pigment-like fluorophores, Free Radic. Biol. Med. 21 (6) (1996) 871–888.
[33] M. Vecellio, F. Spallotta, S. Nanni, et al., The histone acetylase activator pentadecylidenemalonate 1b rescues proliferation and differentiation in the human cardiac mesenchymal cells of type 2 diabetic patients, Diabetes 63 (6) (2014) 2132–2147.
[34] X.W. Cheng, G.P. Shi, M. Kuzuya, et al., Role for cysteine protease cathepsins in heart disease: focus on biology and mechanisms with clinical implication, Circulation 125 (12) (2012) 1551–1562.
[35] S. Aits, J. Kricker, B. Liu, et al., Sensitive detection of lysosomal membrane permeabilization by lysosomal galectin puncta assay, Autophagy 11 (8) (2015) 1408–1424.
[36] R.I. Morimoto, A.M. Cuervo, Proteostasis and the aging proteome in health and disease, J. Gerontol. A Biol. Sci. Med. Sci. 69 (Suppl. 1) (2014) S33–S38.